JVC

Journal of Vibration and Control
000(00) 1–18

DOI: 10.1177/1077546309349851
jvc.sagepub.com
SAGE

# Analysis of crack formation in T-joint structures under dynamic loading

**V N Pilipchuk and R A Ibrahim**

**Abstract**

T-joints play a vital role in the hulls of ships and bulkheads made of sandwich materials. Their design aspects and crack detection are important in preserving the safety of ships navigating through violent sea waves. In this work, an overview of the state-of-the-art of design aspects of T-joints used mainly in ship structures is first provided. The design aspects are focused on estimating static and quasi-static failure loads, fracture and fatigue characteristics. This study also develops a reduced order dynamic model for identification of cracks in T-joints. The reduced model constitutes three modal equations with piecewise-linear asymmetric characteristics in which the influence of the crack appears in terms of its length parameter. In particular, it is shown that the presence of a crack essentially affects both the amplitude and frequency content of the dynamic response due to nonlinear coupling between normal modes. Under external dynamic loading with a frequency close to the first mode frequency, the development of a crack is identified by the evolution of attractors on the configuration planes created by different combinations of modal coordinates.

**Keywords**

Crack detection, nonlinear normal modes, piecewise linear systems, T-joint

Date received: 2 June 2009; accepted: 9 August 2009

## 1. Introduction

### *1.1. Preliminary*

Joints and fasteners are used to transfer loads from one structural element to another in naval vessels, aerospace structures, road vehicles, etc. With reference to composite structures, there are two types of joints commonly used, namely, mechanically fastened joints and adhesive bonded joints. Fastened joints include bolts, rivets, and pins. Adhesive joints depend on the size of the parts to be joined and the amount of overlap that is needed to carry the load. Adhesive joints are often acceptable for secondary structures, but are generally avoided in primary structures on account of strength, chemical interaction effects, and reliability. Bolted joints are still the dominant fastening mechanism used in joining primary structural parts made of advanced composites. The complex behavior of connecting elements plays an important role in the overall dynamic properties such as natural frequencies, mode shapes, and response characteristics to external excitations. The joint represents a discontinuity in the structure and results in high stresses that often initiate joint failure. The stresses and slip in the vicinity of contact regions determine the static strength, cyclic plasticity, frictional damping, and vibration levels associated with the structure (Ibrahim and Pettit, 2005). The following subsections address different issues related to T-joints commonly used in ship structures made of sandwich panels.

### *1.2. Design aspects*

In the composite structures of a ship, the hull and bulkhead are the primary structures in maintaining the ship's stiffness under various loadings. Sandwich panels constitute a major structural element in both hull and bulkhead. These elements consist of two stiff skin sheets and a relatively weak, but lightweight core. For example, a typical joint between the hull and bulkhead used in mine-countermeasure-vessels (MCMVs) is the T-joint. The T-joint consists of composite over-laminates

Department of Mechanical Engineering, Wayne State University, Detroit, MI, USA

**Corresponding Author:**
R A Ibrahim, Department of Mechanical Engineering, Wayne State University, Detroit, MI, USA
Email: ibrahim@eng.wayne.edu

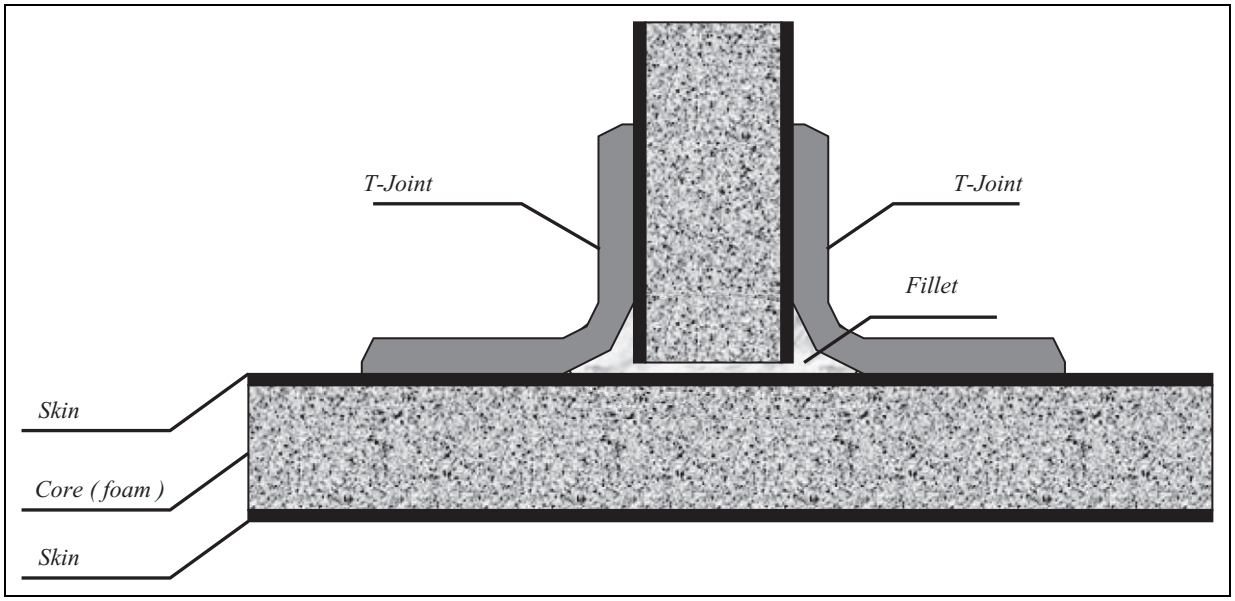


**Figure 1.** T-joint.

to form a large fillet as shown in Figure 1. The function of the T-joint is to transmit flexural, shear, and tensile/compressive loads from one panel (web) to the other (flange). Numerical and experimental studies have been reported in the literature dealing with different aspects of the design and behavior of T-joints (see, e.g., Burchardt, 1995; Theotokoglou and Moan, 1996; Shenoi et al., 1998; Read and Shenoi, 1999; and Turaga and Sun, 2000). Junhou and Shenoi (1996) reviewed the performance characteristics of joints in fiber-reinforced plastic (FRP) marine structures, while the composite materials used in ship structures are reviewed by Mouritz et al. (2001).

In view of the relatively low modulus of FRP material, Dodkins et al. (1994) discussed the problems with forming efficient joints between the major structural components of FRP ships and boats with stiffened single-skin construction ships. They considered T-joints between watertight bulkheads and shell plating and attachment of top-hat stiffeners to plating. The specific stiffness of FRP is in the range of a third to a quarter of the value of metals as shown by Shenoi and Hawkins (1995). One approach used to stiffen fiber-reinforced plastic (FRP) plates is a top-hat stiffener. Kesavan et al. (2006) developed a global neural network architecture incorporating sequential processing of internal sub-networks (GNAISPIN) to predict the presence of multiple damage zones across a structure, made from glass-fiber-reinforced plastic (GFRP). Finite element models of T-joints, used in ship structures, were created with delaminations embedded at various locations across the bond-line of the structure. The resulting strain variation across the surface of the structure was verified experimentally. GNAISPIN was then used in tandem with the damage relativity analysis technique to predict and estimate the presence of multiple delaminations.

Design aspects of T-joints in single-skin FRP ships and boats were discussed by Hawkins et al. (1993) and Toftegaard and Lystrup (2005). Maneepan et al. (2005) studied the optimization of FRP top-hat stiffened single-skin and monocoque sandwich plates subject to a lateral pressure load. They considered plates made of E-glass/epoxy, high-strength carbon/epoxy and ultrahigh-modulus carbon/epoxy. Seven different T-joint sandwich designs made of balsa wood cores and carbon-fiber-reinforced polymer (CFRP) facings were compared under quasi-static tensile and compressive loading until failure by Brunner and Paradies (2000). The performance of the designs is assessed based on failure loads and deformations, acoustic emission (AE) data and visual inspection. The design improvements yield an increase of the failure load from around 50 kN to at least 140 kN (corresponding to the failure of the horizontal plate). AE monitoring revealed an early onset of damage and significant damage accumulation at loads around 70% of the ultimate failure load. For some T-joints there are indications of significant damage in zones outside the region of the final failure. Eksik et al. (2007a, b) experimentally and numerically examined the behavior of a top-hat-stiffened panel under uniform lateral pressure. They developed a finite element model based on an ANSYS three-dimensional solid element (SOLID45) to determine the static response of a top-hat-stiffened panel under uniform lateral pressure. The numerical modeling results were compared to the experimental findings for validation and to further understand an internal stress pattern within the different constituents of the panel for explaining the likely causes of panel failure.

## *1.3. Transverse stitched T-joints*

The mechanical behavior of transverse stitched T-joints using a fiber insertion process and PR520 toughened epoxy

resin under bending and tensile loading was examined by Stickler and Ramulu (2001). Experimental tests were conducted to determine the modes of failure and ultimate failure strength for each load condition. The results indicated that the flexural specimens fail in part from unsymmetrical loading of the fiber insertions and in part from high stress concentration in the " resin-rich" fillet region. Tensile specimens have symmetric loading of both sets of fiber insertions and initially fail due to matrix cracking at the web-to-flange interface. Later, Stickler and Ramulu (2002) examined the effects of key parameters of T-joints with transverse stitching under flexure, tension, and shear loading using finite element analysis. These parameters include fiber insertion tow modulus, fiber insertion filament count, fiber insertion depth, and resin-rich interface zone thickness on T-joint displacement and damage initiation load. It was found that under flexural loading, increasing the fiber insertion tow modulus and tow filament count increases the T-joint damage initiation load. On the other hand, increasing the fiber insertion depth reduces T-joint deflection. Furthermore, reducing the web-to-flange interface thickness reduces the T-joint deflection. The fiber insertion tow filament count and modulus were found to have a negligible effect on T-joint deflection under tension and initial damage load under shear. The progressive damage of a new type of composite T-joint with transverse stitching using a fiber insertion process was modeled using numerical methods by Stickler and Ramulu (2006). They also conducted a series of experiments to determine the load-displacement and strain-load history under flexure and tensile loading. Experimental observations of initial failure were manifested by a discrete drop in the load-displacement behavior and the initiation and propagation of an interfacial matrix crack at the web-to-flange interface. Fiber insertion bridging and fiber insertion breakage were observed at T-joint ultimate failure.

T-joints and top-hat stiffeners create a potential zone of weakness in ships. The mechanical behavior of such structures has been documented in the literature (see, e.g., Phillips and Shenoi, 1998; and Phillips et al., 1999). It was reported that delamination induced damage in the root of the T-joint is a potential source of catastrophic failure. The load transfer mechanisms in single-skin T-joints were examined by Phillips and Shenoi (1998) in terms of the strain energy release rate and the J-integral. The J-integral is a path independent line integral, which measures the magnitude of singular stresses and strains near a crack tip and is based on the concept of energy balance. The fracture mechanics revealed that deep cracks give greater values of the J-integral than surface cracks and long straight cracks give greater values of the J-integral than short straight cracks. Later, the damage tolerance of a top-hat stiffener to plate connection in FRP marine structures was examined by Phillips et al. (1999) who used stress-based and fracture-dependent criteria. Numerical modeling was used to determine the internal load transfer characteristics and failure mechanisms in top-hat stiffeners under static loading. The estimated fracture parameters with regard to delamination in the top-hat over-laminates revealed that delaminations propagate under a straight pull-off load.

Theotokoglou (1997) examined the nonlinear deflection response of highly stressed sandwich T-joints using large deflection and plasticity analyses. The finite element algorithm was based on a plane model of the joint and accounted for plastic deformation of the core and geometric nonlinear effects. The algorithm was also used to identify internal stress states, in various regions of the joint and for different attachment configurations, leading to a failure. Later, Theotokoglou (1999) numerically estimated the J-integral in studying the fracture mechanics of sandwich T-joints formed by two panels connected by lap joints subjected to lateral loads. Kumari and Sinha (2002) studied the static behavior of composite T-joints made of carbon-fiber composite (CFC) materials. A pull-out force was applied to the top of the web to determine the strength of the T-joints. Parametric variations account for two different stacking sequences and variations in filler area and radius of curvature at the web/skin interface.

The fracture behavior of glass-fiber-reinforced polymer (GFRP) T-joints was studied by Dharmawan et al. (2004) and Li et al. (2006) using finite element analyses and the virtual crack closure technique. The structure analyzed contained initial disbond in various locations with various sizes under a straight pull-off load. The strain energy release rate at the disbond tips was used to predict the failure loads and crack growth mechanism of the structure. It was found that skewed loading affected the strain energy release rate at the crack tips, which altered the fracture behavior of the structure. The effect of T-joint geometry on the strain distribution showed that the critical strains were significantly affected by the joint geometry. The results of the finite element analysis revealed that particular defects led to large changes in the strains in the T-joint structure, which would enhance disbond progression. Dharmawan et al. (2008) employed the crack tip element method for damage prediction of the T-joint. This method was found to be an excellent damage prediction tool for composite laminates where an oscillatory singularity exists at the crack tip.

Turaga and Sun (2000) outlined various modes of failure of different T-joints of composite sandwich panels. The key modes of failure include debonding between the two sandwich components to be joined, debonding between the attachment and the sandwich panel, and cracking in the core of the sandwich. A new type of T-joint incorporating an aluminum U-channel in the web sandwich was found to provide much improvement over the conventional circular fillet T-joint. It was shown that using bolts in a circular fillet joint could cause early failure in the core and would not help much to increase the ultimate joint strength. The experimental failure modes of the tested joints were explained with the help of finite element analysis.

### 1.4. Fatigue behavior of T-joints and crack detection

The fatigue behavior of out-of-plane bonded and laminated connections in structures made from fiber-reinforced plastic (FRP) composite materials was studied by Read and Shenoi (1999). The major effects of fatigue include stiffness degradation, residual strength and energy dissipation characteristics. Cheng et al. (1999) presented an experimental study of fatigue crack initiation and growth in tubular T-joints, simulating the extreme case of those used for offshore platforms. The crack locations and profiles were recorded and fractographic examinations were carried out to reveal the mechanisms of crack initiation, growth, and crack closure. The variations in the static strains caused by the formation and growth of cracks were correlated with fatigue cycles by a characteristic equation.

Nwosu et al. (1996) studied the vibration response of tubular T-joints in order to detect cracks along their intersections using the ABAQUS finite element program. Frequency response functions were obtained for a joint with and without cracks. The joint was modeled by 8-node degenerate shell elements having five degrees of freedom per node. Line spring elements were used to model the crack. The exact crack configuration (semi-elliptical shape), as observed from numerous experimental fatigue crack investigations at the critical location, was achieved through a mapping function. The natural frequency changes with respect to crack depth revealed little changes, being 4.82% for a 83% crack depth for the first mode. However, significant changes were observed for bending moment and curvature as a function of crack depth. For an 83% chord thickness crack, a 97% change in bending moment was found at points around the crack vicinity. It was also found that there was a 34.15% to 78% change in bending moments for those locations far away from the crack location. The presence of the crack can be detected at locations far away from the crack location using such sensors as strain gages. Zhou et al. (2008) considered the influence of dynamic loads on the behavior of composite sandwich T-joints commonly used in large panels for naval applications. The results of experimental measurements were used to validate the results of a three-dimensional numerical model simulating the damage processes in sandwich T-joints. The failure load predicted by the finite element analysis was found to be within 30% of the experimental results. The failure modes of the T-joints were found to be sensitive to the core shear failure strength of the base panel. A larger fillet radius helped to increase the failure loads of the T-joint. For example, an increase of the fillet radius of 57% resulted in a 53% increase in the failure load. Fabrication defects were found to significantly reduce the strength of the T-joint with voids between the leg panel and the fillet causing a 37-50% reduction of the failure load.

Bhattacharya et al. (2000) proposed viscoelastic inserts with the purpose of absorbing the vibration in composite joints. The viscoelastic material was arranged as an interlayer in a composite top-hat stiffener. Blake et al. (2001) used a progressive damage model in studying the static structural response of a composite T-joint containing a viscoelastic insert, which acts as a means of attenuating noise and vibration across the joint. The application of a progressive damage model allows the initiation and progression of failure and ultimate failure load to be predicted.

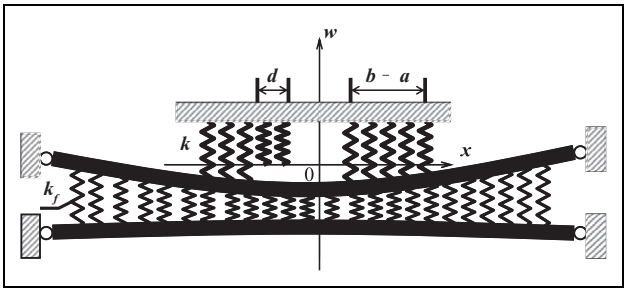


**Figure 2.** Elastic spring model of a joint.

### 1.5. Scope of the present study

This paper presents an analytical approach for a T-joint experiencing crack formation. The analysis is based on representing the main sandwich panel by two outer skins, with the core between them represented by a set of parallel springs. The two legs of the T-joint are also represented by an equal number of springs with one cracked side. For perfect and ideal adhesion of the joint, the springs are in complete contact with the main panel. However, the initiation of a crack is manifested by the disconnection of some springs from one side as shown in Figure 2. It will be shown that the disconnection of springs makes the model physically nonlinear. The main objective of this study is to find out how the linear normal modes (under the no-crack condition) will be affected by the crack as it develops and therefore that the dynamics becomes increasingly nonlinear.

Three different types of representation are used for tracking the system's dynamic properties as the crack develops from a very small initial fracture to almost complete separation of one side of the T-joint. These are configuration planes, response time history records, and Fourier spectrograms. As mentioned earlier, the analytical modeling is based on representing cracks by such elastic elements that work normally in compression phases but show no resistance to tension. Note that such an approach is quite common in the reduced order modeling of cracked elastic structures (see, e.g., Chen and Shaw, 1996; Chati et al., 1997; Butcher, 1999; Jiang et al., 2004; Andreaus et al., 2007; Vestroni et al., 2007; Butcher and Lu, 2007; and Pilipchuk, 2009). However, as shown in Sections 2 and 3, the geometrical specifics of T-joints require the additional

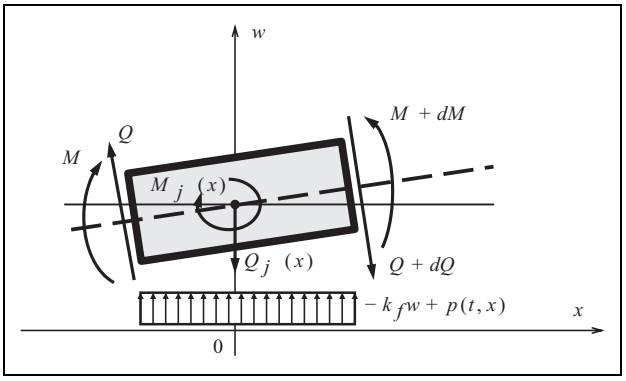


**Figure 3.** A small segment of the beam including the localized joint.

analytical tools of dynamic modeling. For instance, a cracked T-joint is reduced to a specific nonlinear element embedded in an elastic beam and is localized at the center of the T-joint. In addition, the crack length is assumed to grow by a smoothed step-wise law with a slow rate as compared to any other temporal scale associated with the model eigenfrequencies and external loading as proposed in Section 6. The model reduction, which is implemented in Section 4, is based on the first three modes of a beam with no joint. As a result, the corresponding differential equations of motion are linearly coupled due to the presence of the joint even though no crack/nonlinearity develops. Furthermore, the system is decoupled in linear coordinates through a principal coordinates transformation of the beam with joint. Such a preliminary adaptation shows one of the possible ways of crack detection by analyzing the system's dynamic response to specific external excitations. In particular, as discussed in Section 6, under the resonance excitation of one of the modes, some other modes may be excited indirectly through the nonlinear coupling generated by the crack. In addition, the frequency content of each individual mode is also affected by the crack due to the presence of nonlinearity. Finally, in Section 7, some conclusions will be made regarding a possible practical use of the developed approach.

## 2. Joint modeling and preliminary remarks

Consider a simplified elastic model of a T-joint initially cracked as schematically shown in Figure 2. The main structure is a sandwich beam whose core is modeled by a set of elastic springs with a distributed stiffness of $k_f$ per unit length. The upper and lower skins are represented by two thin beams each of length $L$, density $\rho$, and bending stiffness $EI$, where $E$ is the Young's modulus and $I$ is the area moment of inertia of the skin cross-section. The reaction of the T-joint attached to the horizontal beam is represented by a continuous set of linearly elastic springs whose distributed stiffness per unit length is $k$ and occupy the

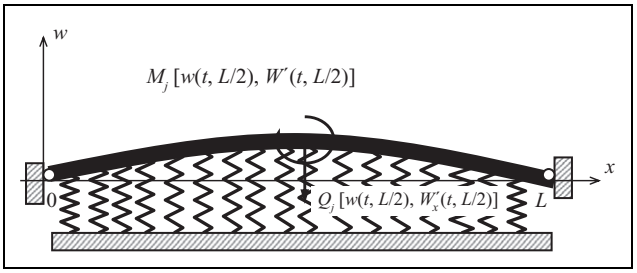


**Figure 4.** Equivalent model for the beam with localized joint.

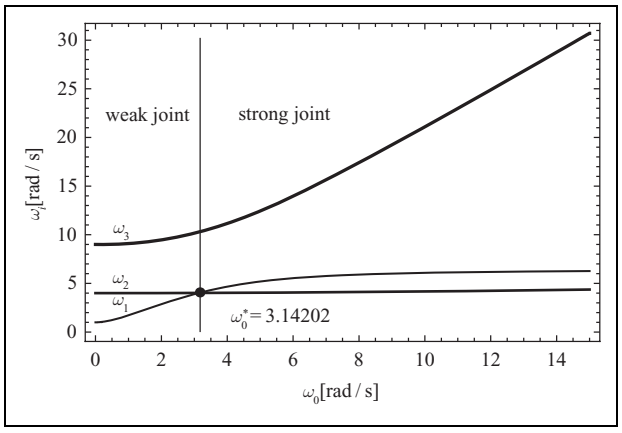


**Figure 5.** Frequency versus the joint strength parameter showing the internal 1:1 resonance between the first two modes; $\omega_0 = \sqrt{2k(b-a)/(AL\rho)}$

region $b - a$ on each leg of the T-joint. In order to simplify preliminary derivations, it is assumed that the perfect (no crack) joint is symmetric with respect to the origin $x = 0$. However, when a small area of separation occurs, the elastic reaction of the joint within the area of separation becomes essentially nonlinear and may be described by the following functions

$$f(x,w) = \begin{cases} kw & x \in [-b,-a-d] \cup [a,b], \\ kH(w)w & x \in [-a-d,-a], \\ 0 & x \notin [-b,-a] \cup [a,b], \end{cases} \quad (1)$$

where $H(\bullet)$ is the unit-step Heaviside function.

Note that the deflection function $w(t,x)$ is associated with the center line of the sandwich or the upper skin beam as follows. In the case of global long-wave modes, when the upper and lower beams vibrate in-phase, the function $w(t,x)$ effectively describes the position of the entire sandwich. However, in this case, the bending stiffness of the upper beam must be replaced by the effective bending stiffness of the sandwich. As an alternative, one can consider such cases when the vibration modes involve mostly the upper beam and the nearest layers of the core material whose effect on the beam can be represented by a specific elastic foundation. Other modes would require a detailed consideration of coupling between the two beams.

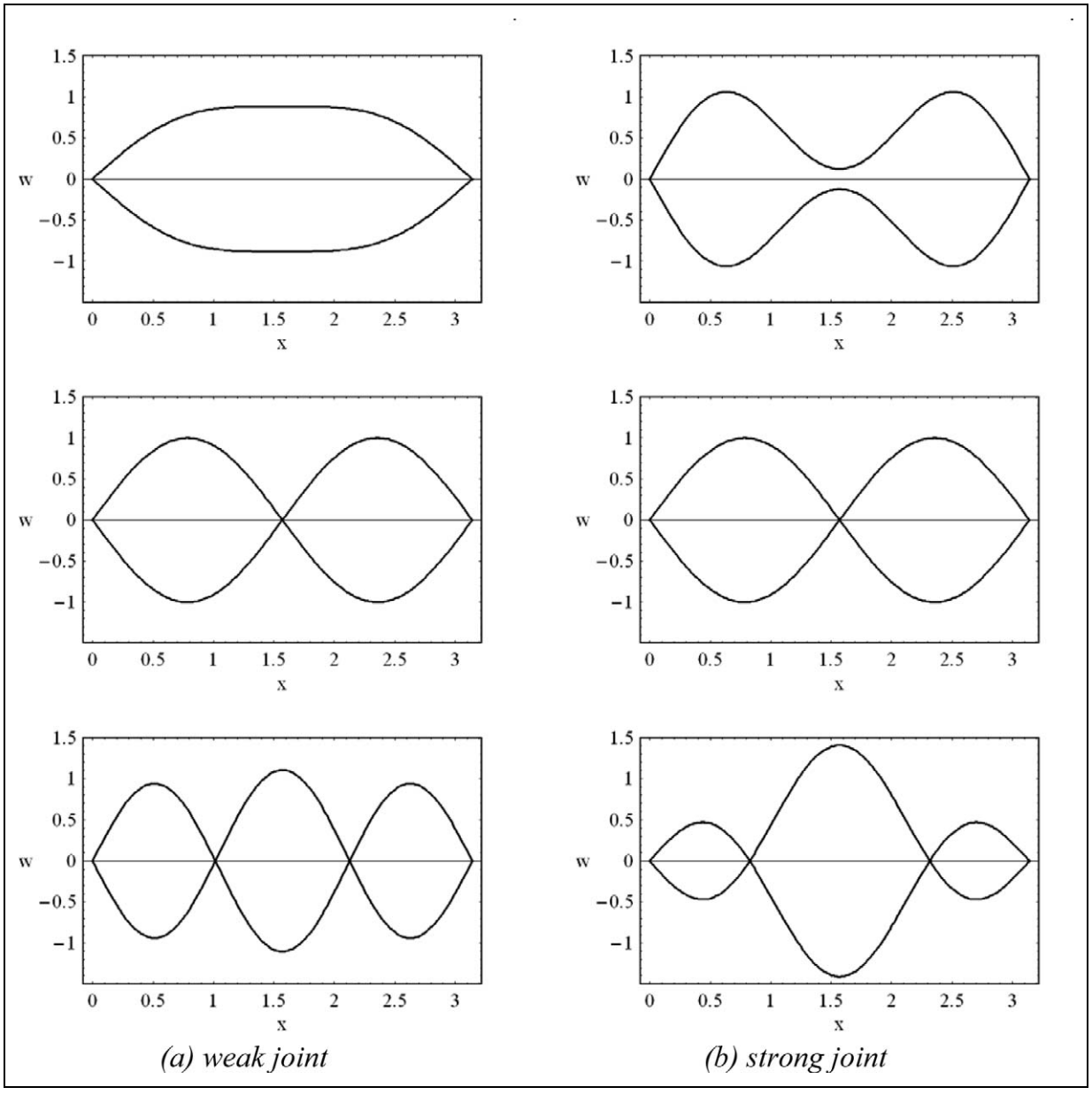


**Figure 6.** First three mode shapes of the beam with a "weak" or "strong" joint.

According to equations (1), there is no interaction between the beam and joint in the area $x \in [-a-d, -a]$ whenever $w(t,x) < 0$. Therefore, for negative deflections of the upper beam, the joint reaction becomes weak and non-symmetric with respect to the origin. On the other hand, when the beam deflection is positive everywhere in the area of joint, then the mechanical properties are equivalent to those of the undamaged joint. Note that, on one hand, such kinds of dynamic behavior bring the model into a class of distributed vibrating systems with nonsmooth nonlinearities, which are quite difficult to analyze (see, e.g., Chen and Shaw, 1996; Chati et al., 1997; Butcher, 1999; Jiang et al., 2004; Andreaus et al., 2007; Vestroni et al., 2007; Butcher and Lu, 2007; and Pilipchuk, 2009). On the other hand, it will be shown shortly that the corresponding characteristics of a nonlinear dynamic response can be employed for damage detection in joints.

Finally, based on the joint modeling given by equation (1), the total transverse force, $Q_j(t)$, and bending moment, $M_j(t)$, applied from the joint to the beam are determined as follows

$$Q_j(t) = \int_{-b}^{b} f(x, w(t,x))\,\mathrm{d}x, \tag{2}$$

and

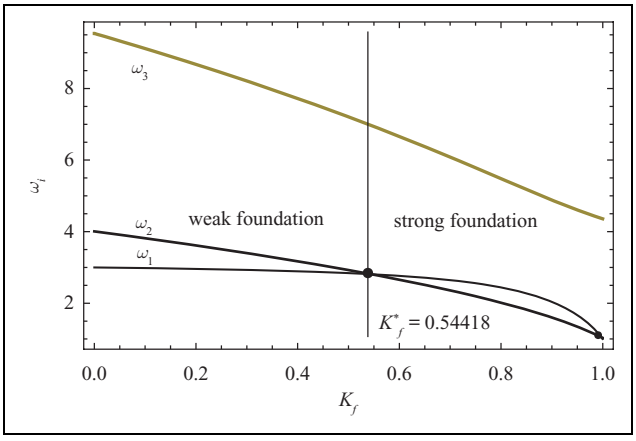


**Figure 7.** Frequency versus foundation stiffness in the weak joint case; $\lambda_1 = 1.0$, $\omega_0 = 2.1213$, $K_f = k_f/(\rho A)$

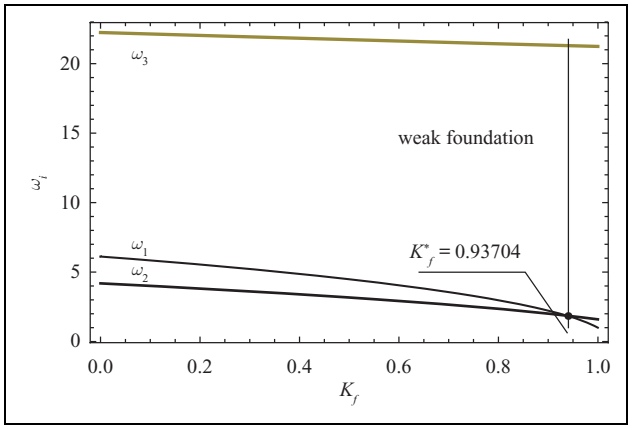


**Figure 8.** Frequency versus foundation stiffness in the strong joint case; $\lambda_1 = 1.0$, $\omega_0 = 10.6066$, $K_f = k_f/(\rho A)$

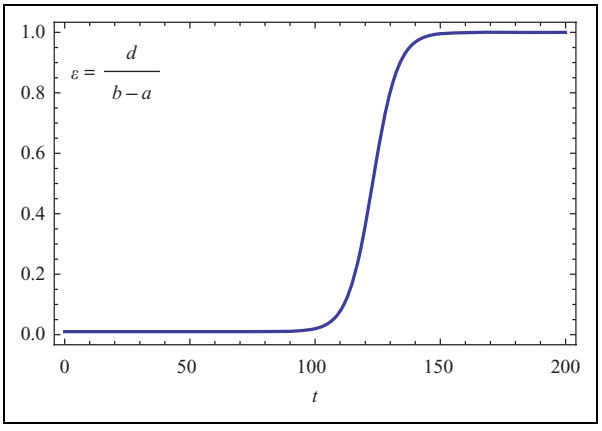


**Figure 9.** The relative length of a crack versus time based on the model adopted.

$$M_j(t) = \int_{-b}^{b} xf(x, w(t,x))\,\mathrm{d}x. \tag{3}$$

At this stage, expressions (2) and (3) cannot be used because the function $w(t,x)$ is *a priori* unknown. Nevertheless, the above expressions may help to facilitate the problem formulation under certain assumptions regarding the function $w(t,x)$ in the area of joint interaction as will be described in the next section.

## 3. Long-wave asymptotics

In view of the relative structural complexity of the T-joint, shown in Figure 1, its dynamic behavior may significantly depend upon spatiotemporal characteristics of external loads. The idea of the model reduction may be contemplated *a priori* to account for possible dynamic modes that may occur under given loading conditions. For nondestructive diagnostic purposes, one may apply necessary dynamic excitations that are capable of generating such modes that exhibit sufficient sensitivity to crack formation.

In particular, one may assume that the elastic dynamic state of the upper beam at any time $t$ is slowly varying with respect to the spatial coordinate $x$ as compared to the area of contact with the joint. Such a dynamic state can occur provided that the horizontal beam is long enough. In this case, the transverse force, given by equation (2), and bending moment, given by equation (3), applied from the joint to the beam can be considered localized at the joint center $x = 0$. In addition, the integrals of equations (2) and (3) admit explicit calculations by using the truncated power series for $w(t,x)$ about the center of the joint, $x = 0$, i.e.,

$$w(t,x) = w(t,0) + w_x'(t,0)x + O(x^2). \tag{4}$$

Equation (4) implies that the function $w(t,x)$ is smooth enough with respect to $x$.

Note that the integrands in both equations (2) and (3) include the nonsmooth function $H(w)w$, which can be approximated, nevertheless, by the generalized power series (see, e.g., Richmyer, 1985),

$$H(w(t,x))w(t,x) = H(w(t,0))[w(t,0) + w_x'(t,0)x] + O(x^2), \tag{5}$$

where the following property of distributions has been taken into account

$$zH'(z) = z\delta(z) = 0. \tag{6}$$

Substituting equation (4) into equations (2) and (3), taking into account equation (1), gives

$$Q_j(t) = 2k(b-a)w(t,0) - kd\Psi(w(t,0), w_x'(t,0)), \tag{7}$$

$$M_j(t) = \frac{2}{3}k(b^3 - a^3)w_x'(t,0) + kda\Psi(w(t,0), w_x'(t,0)), \tag{8}$$

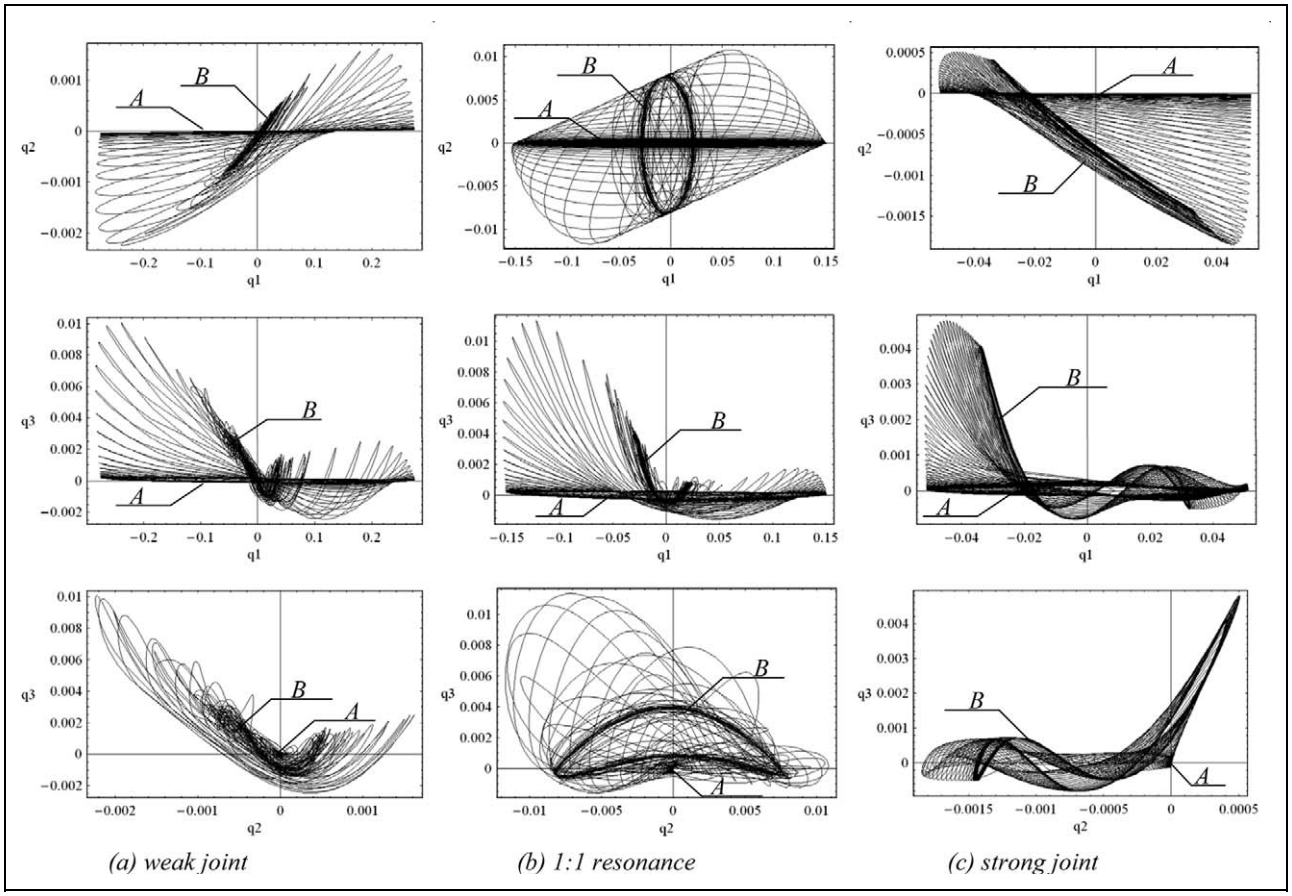


**Figure 10.** Projections of the system trajectory on configuration planes in three different cases of the joint stiffness under the developing fracture condition and loading $p_1 = 0.1 \sin \omega_1 t$, $p_2 = p_3 = 0$: A – initial crack, and B – developed crack.

where

$$\psi(z_1, z_2) = [1 - H(z_1)](z_1 - az_2). \tag{9}$$

In order to incorporate the localized force and moment, given by equations (2) and (3), into the model, consider a small segment of the beam as shown in Figure 3.

Following the classic approach and ignoring the angular inertia force, gives the following balance of forces and moments

$$\rho A\,\mathrm{d}x \frac{\partial^2 w}{\partial t^2} = Q - (Q + \mathrm{d}Q) + [p(t,x) - k_f w - Q_j \delta(x)]\,\mathrm{d}x, \tag{10}$$

$$0 = -M + (M + \mathrm{d}M) - M_j \delta(x)\,\mathrm{d}x - \frac{1}{2} Q\,\mathrm{d}x - \frac{1}{2}(Q + \mathrm{d}Q)\,\mathrm{d}x, \tag{11}$$

where $\rho$ is the mass density of the beam, $A$ is the cross-sectional area, and $k_f$ characterizes the distributed elastic properties of the foundation represented by a continuous set of linearly elastic springs.

Eliminating the high-order term $\mathrm{d}Q\,\mathrm{d}x$ from equation (11), and dividing both sides of the equations by $\mathrm{d}x$, gives

$$\rho A \frac{\partial^2 w}{\partial t^2} = -\frac{\partial Q}{\partial x} - Q_j \delta(x) - k_f w + p(t,x), \tag{12}$$

$$Q = \frac{\partial M}{\partial x} - M_j \delta(x), \tag{13}$$

where

$$M = EI \frac{\partial^2 w}{\partial x^2}. \tag{14}$$

Figure 4 shows the upper skin represented by a simply supported beam of length $L$ by assuming that the joint is localized at the middle of the beam, $x = L/2$. Substituting equations (13) and (14) into equation (12), gives the partial differential equation of motion for the beam's center line in the form

$$\rho A \frac{\partial^2 w}{\partial t^2} + EI \frac{\partial^4 w}{\partial x^4} + k_f w + Q_j \delta\left(x - \frac{1}{2}L\right) - M_j \delta'\left(x - \frac{1}{2}L\right) = p(t,x), \tag{15}$$

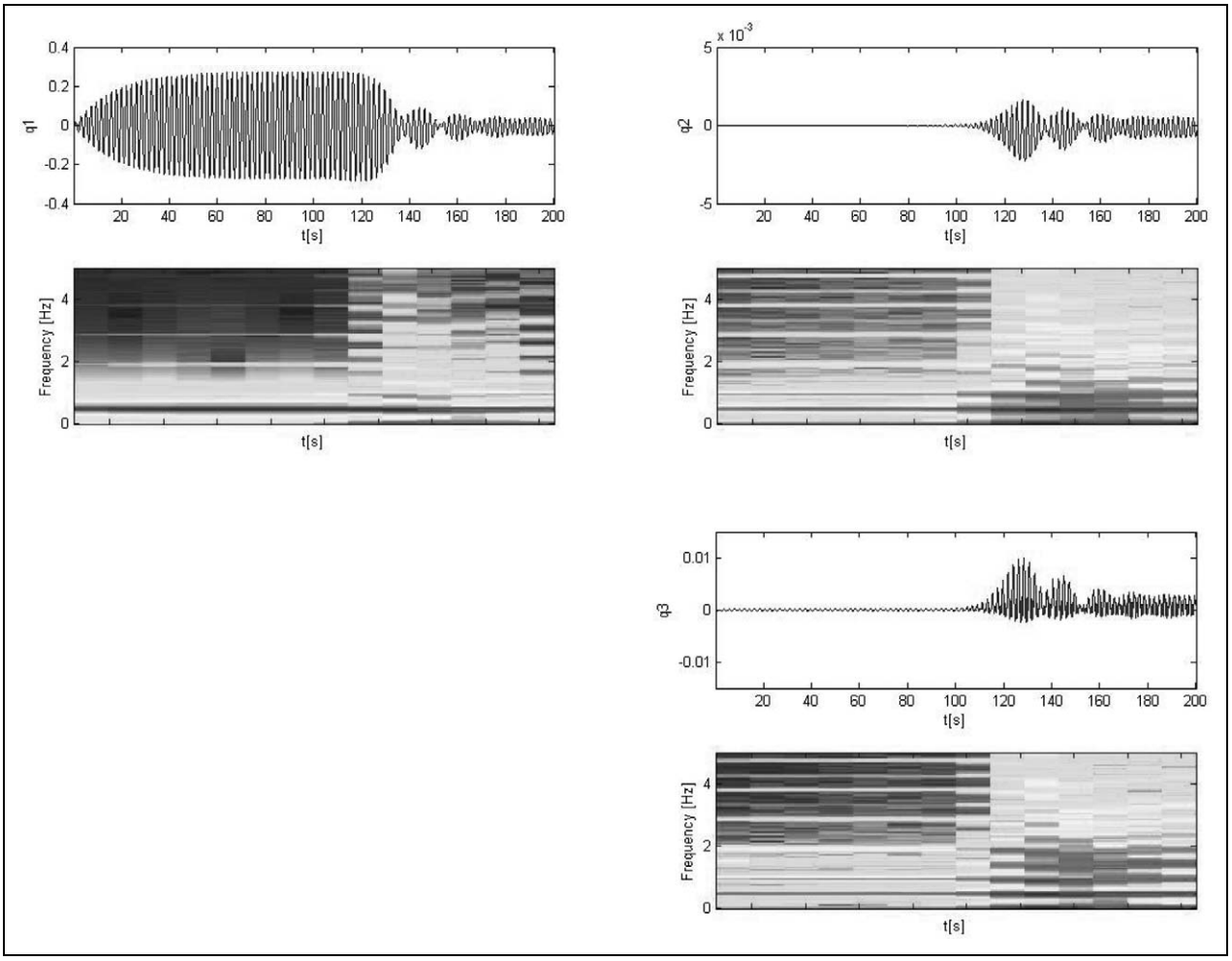


**Figure 11.** Time history records and the corresponding spectrograms for the modal coordinates in the case of a weak joint under the developing fracture condition and first linear mode resonance excitation (relates to Figure 10(a)).

where

$$Q_j(t) = 2k(b-a)w(t,L/2) - kd\Psi(w(t,L/2), w_x'(t,L/2)), \tag{16}$$

$$M_j(t) = \frac{2}{3}k(b^3-a^3)w_x'(t,L/2) + kda\Psi(w(t,L/2), w_x'(t,L/2)). \tag{17}$$

Equation (15) is subject to the boundary conditions

$$w(t,x)|_{x=0,L} = 0,$$

$$\frac{\partial^2 w(t,y)}{\partial x^2}|_{x=0,L} = 0. \tag{18}$$

Note that as a joint crack develops (i.e., $d > 0$), the model described by equations (15) through (18) becomes nonlinear such that the strength of nonlinearity is proportional to the length of the crack $d$. As stated in the introduction, one of the main objectives of this study is to find out how the linear normal modes (under the no-crack condition $d = 0$) will be affected by the crack as its size $d$ increases. The cases of free and forced vibrations of the beam will be considered below in order to clarify the influence of crack formation on the beam's response in both cases.

## 4. Discretization and modal analysis

Following the idea of the Bubnov-Galerkin method, the beam center line and external loading functions are represented as a linear combination of the first three mode shapes of the beam with no joint attached

$$w(t,x) = \sum_{i=1}^{3} w_i(t)\sin\frac{i\pi x}{L}, \tag{19}$$

$$p(t,x) = \rho A\sum_{i=1}^{3} p_i(t)\sin\frac{i\pi x}{L}, \tag{20}$$

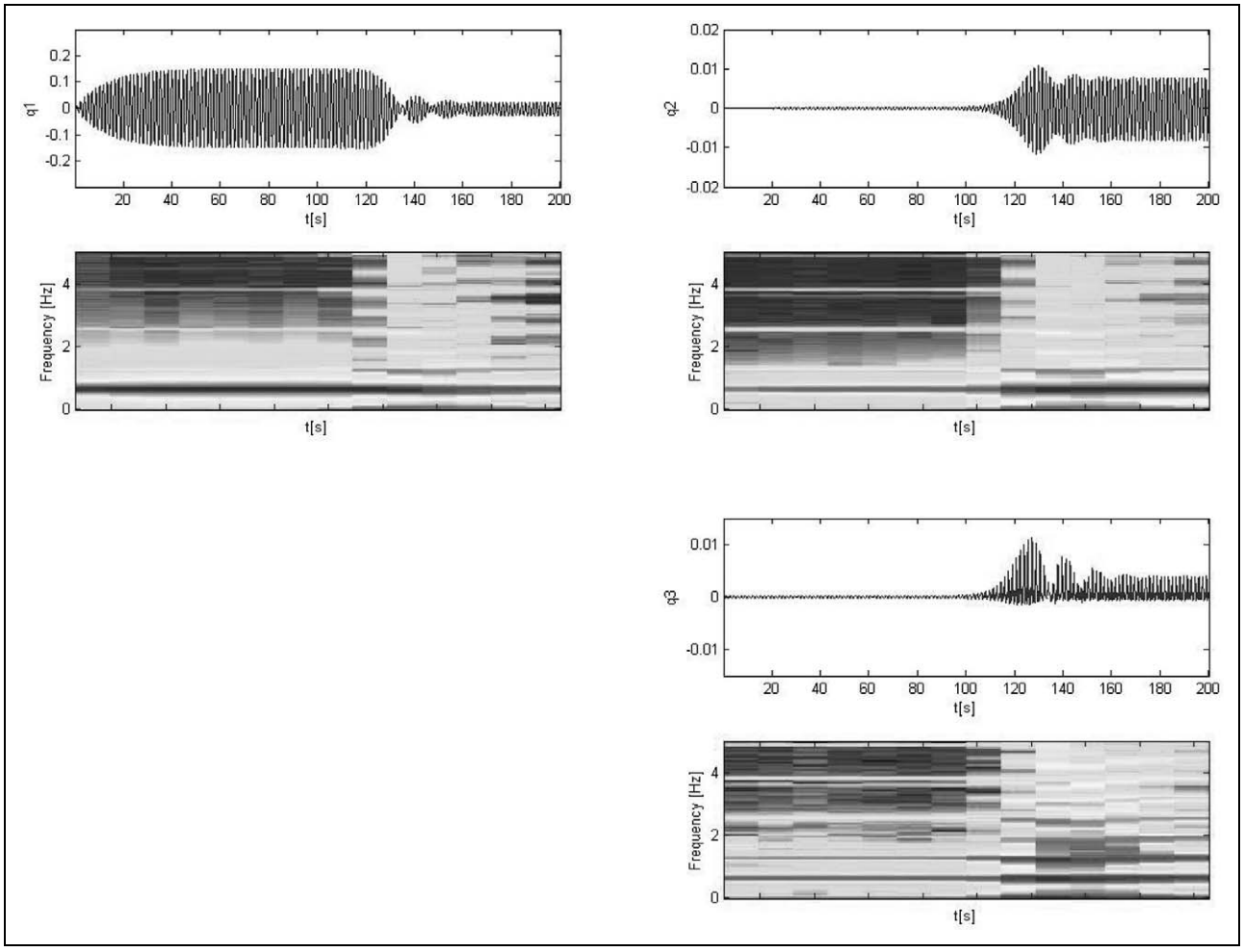


**Figure 12.** Time history records and the corresponding spectrograms for the modal coordinates in the case of 1:1 resonance under the developing fracture condition and first linear mode resonance excitation (relates to Figure 10(b)).

where $\rho A$ is the beam mass per unit length, which is introduced as a scaling factor of the external loading function in order to simplify further notations.

Substituting equations (19) and (20) into equation (15) and applying the Bubnov-Galerkin procedure, gives the following three equations of motion in terms of the generalized coordinates $w_i(t),\ i = 1, 2, 3,$

$$\begin{aligned}
&\ddot{w}_1 + \lambda_1^2 w_1 + 2\omega_0^2(w_1 - w_3) \\
&- \varepsilon\omega_0^2 F(w_1 - w_3, w_2) = p_1(t), \\
&\ddot{w}_2 + \left[\lambda_2^2 + \frac{8}{3}(r_a^2 + r_a r_b + r_b^2)\omega_0^2\right] w_2 \\
&- 2\varepsilon r_a \omega_0^2 F(w_1 - w_3, w_2) = p_2(t), \\
&\ddot{w}_3 + \lambda_3^2 w_3 - 2\omega_0^2(w_1 - w_3) \\
&+ \varepsilon\omega_0^2 F(w_1 - w_3, w_2) = p_3(t),
\end{aligned} \tag{21}$$

where $\lambda_j = \sqrt{[k_f + EI(j\pi/L)^4]/(\rho A)}$ are the eigenvalues of the beam setting on an elastic foundation with no joints, $\omega_0 = \sqrt{2k(b-a)/(AL\rho)}$ is the natural frequency of an oscillator whose mass is equal to the mass of the beam, where the stiffness is equal to the total stiffness of the joint, $r_a = \pi a/L$ and $r_b = \pi b/L$ are nondimensional geometrical parameters characterizing the size of the joint, and $\varepsilon = d/(b-a)$ is a parameter characterizing the size of the crack. The nonlinearity due to the crack may be described by the nonsmooth function

$$\begin{aligned}
F(w_1 - w_3, w_2) &= F(z_1, z_2) \\
&= [1 - H(z_1)](z_1 + 2r_a z_2),
\end{aligned} \tag{22}$$

where $z_1 = w_1 - w_3$ and $z_1 = w_2$.

In the absence of a joint we have $\omega_0 = 0$ and thus equations (21) exactly describe the behavior of the first three linear normal modes of the beam. In the presence of the joint with no crack, however, we have $\omega_0 \neq 0$ but $\varepsilon = 0$. In this case, equations (21) are still linear, but $w_1(t)$ and $w_3(t)$ are not the principal coordinates any more. To this end it is convenient to introduce a transformation of the principal coordinates, $q_i,\ i = 1, 2, 3,$ of the linearized

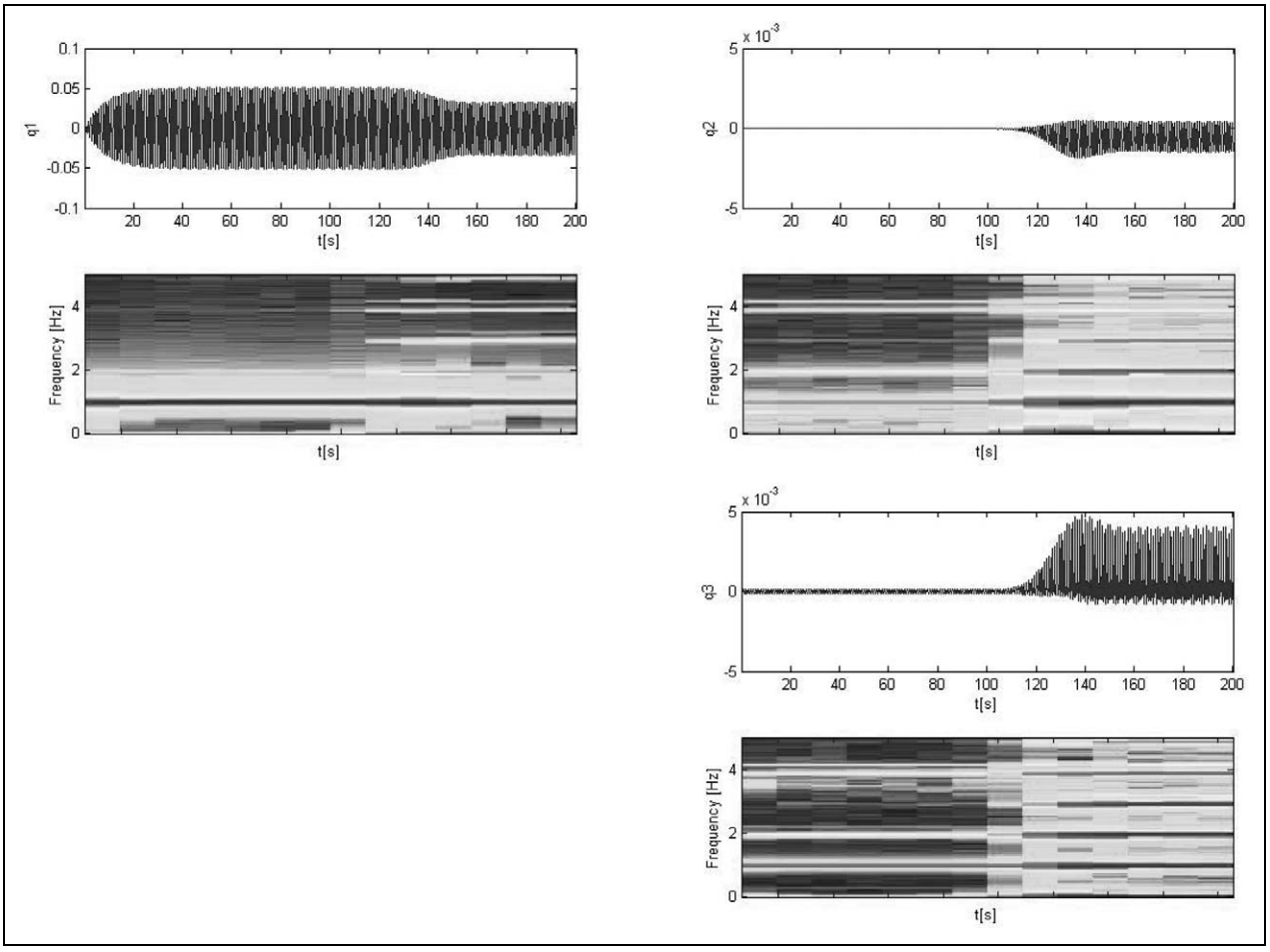


**Figure 13.** Time history records and the corresponding spectrograms for the modal coordinates in the case of a strong joint under the developing fracture condition and first linear mode resonance excitation (relates to Figure 10(c)).

perfect system (with no crack, $\varepsilon = 0$) (21)

$$
\begin{aligned}
w_1(t) &= \frac{\sqrt{2}}{2}\left(\sqrt{r_1^2 + r_2^2 + r_2}\,q_1(t) - \sqrt{r_1^2 + r_2^2 - r_2}\;q_3(t)\right),\\
w_2(t) &= q_2(t),\\
w_3(t) &= \frac{q_1(t)}{\sqrt{1 + (1 + r_2)^2/r_1^2}} + \frac{q_3(t)}{\sqrt{1 + (1 - r_2)^2/r_1^2}},
\end{aligned}
\tag{23}
$$

where the second mode remains the same since it is already decoupled from the other two modes of the linearized model ($\varepsilon = 0$), and the parameters of transformation are expressed through the natural frequencies $\omega_1$ and $\omega_3$ as $r_1 = 4\omega_0^2/(\omega_3^2 - \omega_1^2)$ and $r_2 = (\lambda_3^2 - \lambda_1^2)/(\omega_3^2 - \omega_1^2)$, and the entire spectrum of the linear model with joint is given by the following expressions

$$
\begin{aligned}
\omega_1^2 &= \frac{1}{2}\left(4\omega_0^2 + \lambda_1^2 + \lambda_3^2 - \sqrt{16\omega_0^2 + \left(\lambda_1^2 - \lambda_3^2\right)^2}\right),\\
\omega_2^2 &= \lambda_2^2 + \frac{8}{3}(r_a^2 + r_a r_b + r_b^2)\omega_0^2,\\
\omega_3^2 &= \frac{1}{2}\left(4\omega_0^2 + \lambda_1^2 + \lambda_3^2 + \sqrt{16\omega_0^2 + \left(\lambda_1^2 - \lambda_3^2\right)^2}\right).
\end{aligned}
\tag{24}
$$

Substituting the transformation (23) into equations (21) and adding an effective damping in a phenomenological way, gives

$$
\begin{aligned}
&\ddot{q}_1 + 2\zeta_1\omega_1\dot{q}_1 + \omega_1^2 q_1 = \varepsilon\Phi_1(q_1, q_2, q_3) + P_1(t),\\
&\ddot{q}_2 + 2\zeta_2\omega_2\dot{q}_2 + \omega_2^2 q_2 = \varepsilon\Phi_2(q_1, q_2, q_3) + P_2(t),\\
&\ddot{q}_3 + 2\zeta_3\omega_3\dot{q}_3 + \omega_3^2 q_3 = \varepsilon\Phi_3(q_1, q_2, q_3) + P_3(t),
\end{aligned}
\tag{25}
$$

where $\zeta_i,\ i = 1, 2, 3$, are modal damping ratios, that will be assumed equal in the numerical simulations,

$$
\begin{aligned}
&\Phi_1(q_1, q_2, q_3) =\\
&-\frac{1}{2}\omega_0^2(1 - r_1 - r_2)\sqrt{1 + (1 + r_2)^2/r_1^2}\;\Phi(q_1, q_2, q_3),\\
&\Phi_2(q_1, q_2, q_3) = 2r_a\omega_0^2\Phi(q_1, q_2, q_3),\\
&\Phi_3(q_1, q_2, q_3) =\\
&-\frac{1}{2}\omega_0^2(1 + r_1 + r_2)\sqrt{2/(1 + r_2)}\,\Phi(q_1, q_2, q_3),
\end{aligned}
\tag{26}
$$

and $\Phi(q_1, q_2, q_3)$ is given by substituting expressions (23)

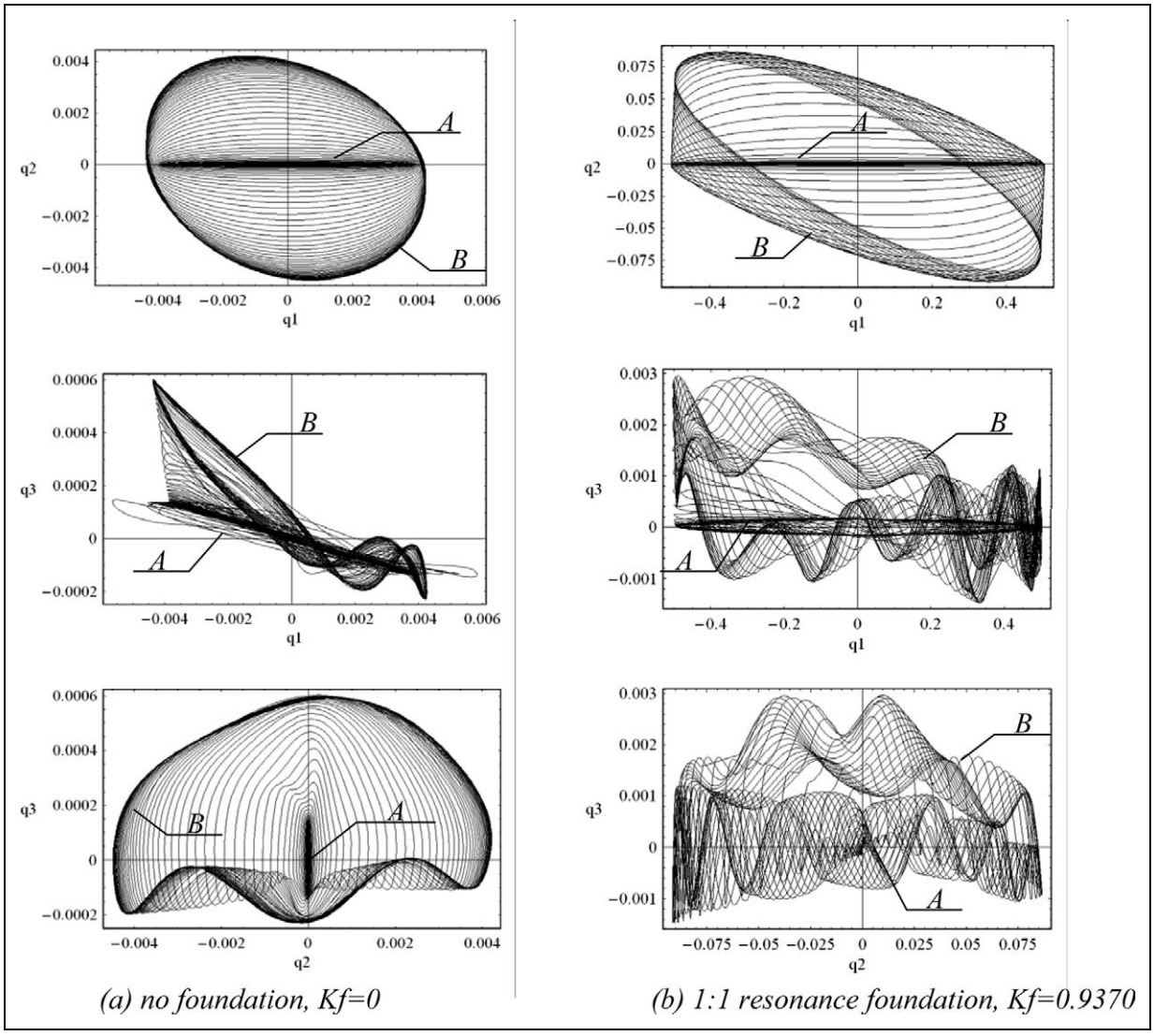


**Figure 14.** Projections of the system trajectory on configuration planes in the strong joint case with stiffness under the developing fracture condition and loading; $p_1 = 0.1 \sin \omega_2 t,\ p_2 = p_3 = 0$.

in $F(w_1 - w_3, w_2)$ as defined by (22), and the following notations for the forcing functions have been introduced

$$P_1(t) = \frac{1}{2}[r_1 p_1(t) + (1 - r_2)p_3(t)]\sqrt{1 + (1 + r_2)^2/r_1^2},$$
$$P_2(t) = p_2(t), \tag{27}$$
$$P_3(t) = \frac{1}{2}[-r_1 p_1(t) + (1 + r_2)p_3(t)]\sqrt{2/(1 + r_2)}.$$

The system of equations (25) becomes completely decoupled in terms of the modal coordinates in the absence of any crack, $\varepsilon = 0$. Therefore, the effect of modal coupling as well as spectral deviations from the frequencies $\omega_1$, $\omega_2$, and $\omega_3$ can be used for the purpose of crack detection.

Note that the modal coordinates $q_1$, $q_2$, and $q_3$ cannot provide an exact description of the beam mode shapes with the middle joint even though no crack developed ($\varepsilon = 0$). This is clear from the fact that the Bubnov-Galerkin procedure for the boundary value problem (15) through (18) was based on the linear combination of mode shapes of the beam without a middle joint as given by equation (19).

## 5. Preliminary frequency estimates

It is known that the spectral properties of linearized vibrating systems, in particular the possibility of the so-called internal resonance conditions, may have a strong effect even on nonlinear dynamics when relatively small nonlinearities are present in the corresponding differential equations of motion. Under fixed material mass densities and geometry, the relationship between the eigenfrequencies of the current model is determined by the beam's bending stiffness, elastic foundation, and joint stiffness.

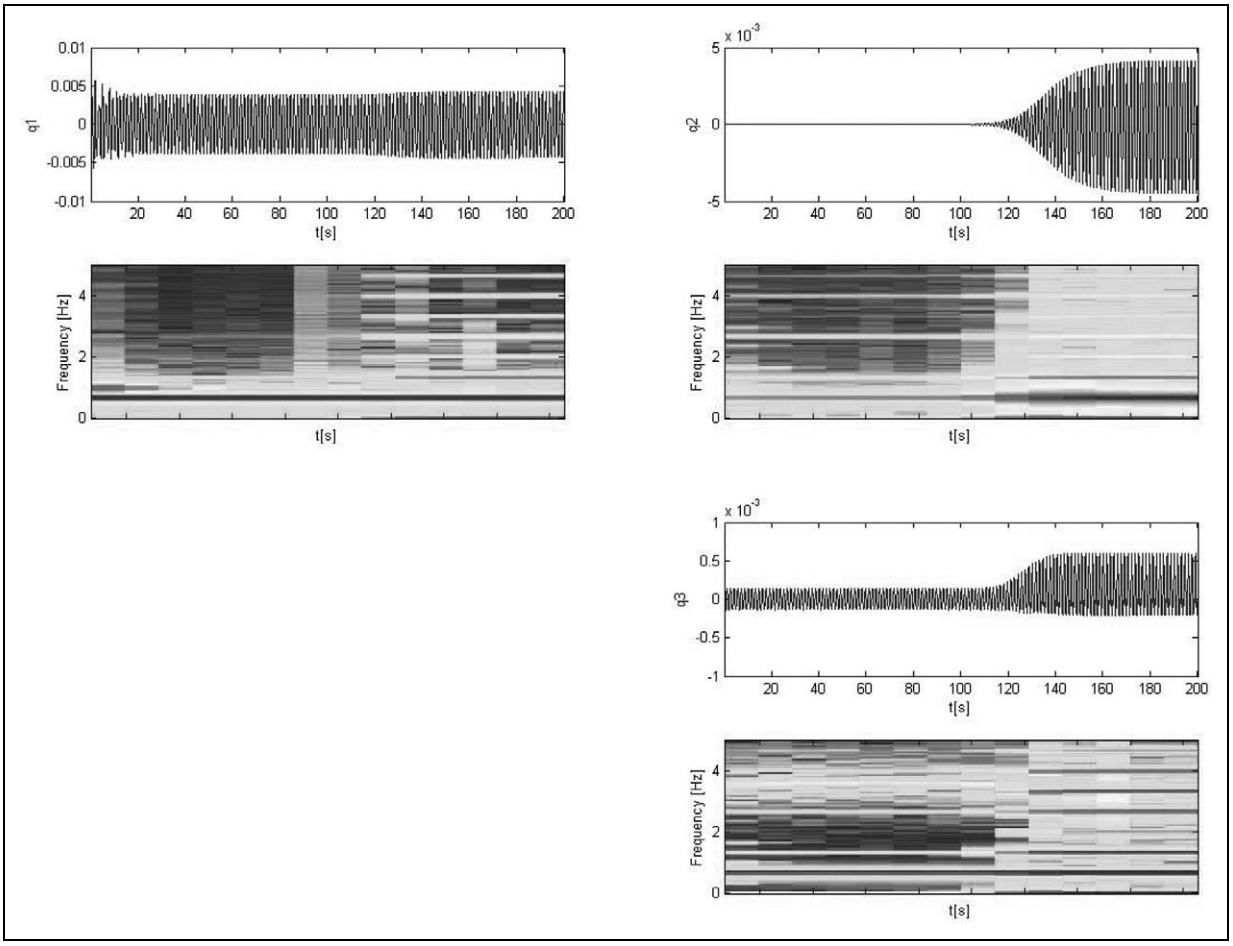


**Figure 15.** Time history records and the corresponding spectrograms for the modal coordinates under the condition of Figure 14(a).

The previous definition of the frequency, $\omega_0$, can be physically viewed as a characteristic parameter representing the strength of the T-joint. For example, Figure 5 illustrates the dependence of the modal frequencies on the joint strength parameter, $\omega_0$. These plots are obtained for the system parameters: $L = \pi$, $r_a = 0.02$, $r_b = 0.06$, $\epsilon = 0.01$, and $\zeta = \zeta_1 = \zeta_2 = \zeta_3 = 0.02$. In order to select a convenient time unit for simulations, the unit frequency is defined by imposing the condition $\lambda_1 = 1.0$, which is equivalent to the following constraint on the parameters

$$\frac{EI}{\rho A} = \left(\frac{L}{\pi}\right)^4 (1 - K_f). \tag{28}$$

Here, $K_f = k_f/(\rho A) = k_f L/(\rho A L) = \omega_f^2$, and thus $\omega_f = \sqrt{K_f}$ is the frequency of an effective oscillator whose mass is the total mass of the beam where its linear stiffness is the total stiffness of the foundation.

At this stage, consider the case of no foundation ($k_f = 0$) so that $EI/(\rho A) = 1.0$.

Figure 5 reveals that 1:1 internal resonance $\omega_1 = \omega_2$ is reached at a critical value of $\omega_0 = \omega_0^* = 3.14202$ [rad/s]. Above this critical value, the frequency of the first mode is larger than the frequency of the second mode. Figure 6 shows two sets of mode shapes belonging to weak [set (a)] or strong [set (b)] joints. Set (a) of Figure 6 illustrates the first three mode shapes for the case of a weak joint ($\omega_0 = 2.12$, $\omega_1 = 3.0$, $\omega_2 = 4.0$, $\omega_3 = 9.5$), while series (b) shows the mode shapes for the case of a strong joint ($\omega_0 = 10.61$, $\omega_1 = 6.12$, $\omega_2 = 4.19$, $\omega_3 = 22.24$). The influence of the joint is manifested in the first mode shape in both weak and strong joints. For the case of a weak joint the first mode shape is flattened over a wide region near the joint. For the case of a strong joint, on the other hand, the first mode shape exhibits a wrinkle near the T-joint. Thus, the point $\omega_0 = \omega_0^*$ can be viewed as a physical boundary between the areas of relatively weak and strong joints.

Further, Figure 7 illustrates the dependence of the spectrum on the foundation stiffness parameter, $K_f$. The point $K_f = K_f^* = \omega_f^{*2}$, at which the internal resonance $\omega_1 = \omega_2$ occurs, can be viewed as a boundary between the areas of weak and strong foundations. Note that, due to the constraint equation (28), the increase of foundation stiffness is accompanied by the decrease of bending stiffness of the

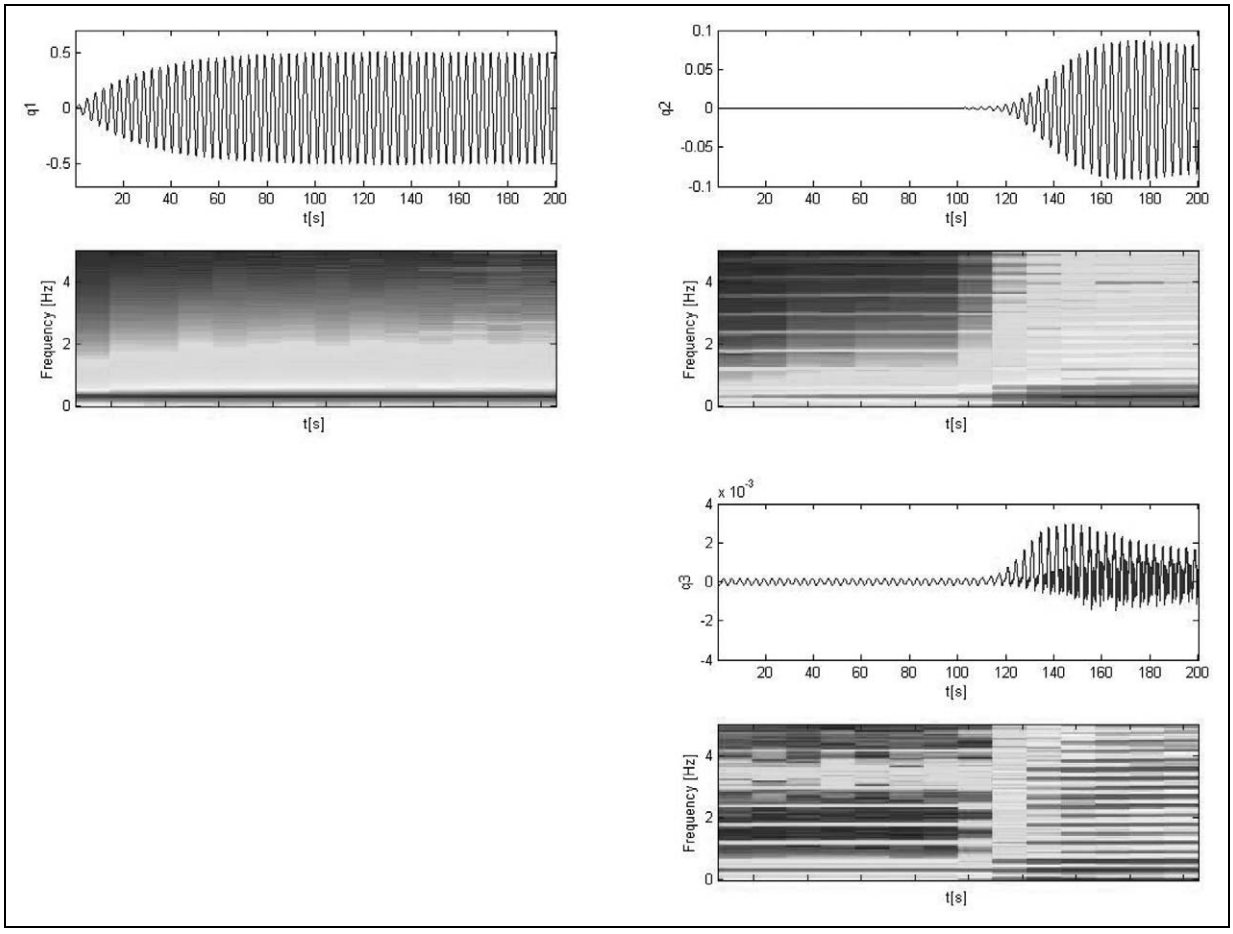


**Figure 16.** Time history records and the corresponding spectrograms for the modal coordinates under the condition of Figure 14(b).

beam. Eventually, at the point $K_f = 1.0$, the beam's bending rigidity vanishes. This is another point of the internal resonance $\omega_1 = \omega_2$, which is possibly beyond the applicability of the model. Indeed, the three-term expansion of equation (19) may not be enough to capture the behavior of mode shapes near the joint as the beam becomes very flexible.

Finally, Figure 8 shows the dependence of the beam modal frequencies on the foundation stiffness $K_f$ for the case of a strong joint. Compared with the case of a weak joint represented by Figure 7, the area of weak foundations is wider. Also, the relationship $\omega_1$ holds on the left-side of the internal resonance $\omega_1 = \omega_2$, so that stronger foundations bring the order of frequencies back to "normal."

## 6. Dynamic response due to crack formation

In order to clarify the evolution of the dynamic response due to crack formation in the joint, the following phenomenological time dependence for the fracture length is assumed

$$\varepsilon = \varepsilon(t) = \varepsilon_0 \varepsilon_\infty \left\{ \varepsilon_0 - (\varepsilon_0 - \varepsilon_\infty) \frac{1 + \tanh[-\lambda_c (t - t_c)]}{1 + \tanh(\lambda_c t_c)} \right\}^{-1}, \tag{29}$$

where $\varepsilon_0$ and $\varepsilon_\infty$ are the initial and final relative fracture lengths as $t = 0$ and $t \to \infty$, respectively; $\lambda_c$ and $t_c$ are parameters characterizing the temporal scale and phase of crack formation.

Figure 9 shows a typical plot of the evolution of the fracture length parameter $\varepsilon$ with time, which also corresponds to the number of cycles. In particular, under specific numerical values of the parameters, such kinds of dependencies can fit experimental data obtained for deterioration of joints under the condition of cyclic loading (see, e.g., Ibrahim and Pettit, 2005). This seems to be a very general smooth approximation for any step-wise behavior. In the present study, the step duration is about 50 time units, that is long enough to cover multiple vibration cycles. At earlier stages, the crack propagation is very slow starting from, initially, a very small relative length parameter $\varepsilon_0 = 0.01$. Then most of the crack formation develops within the time

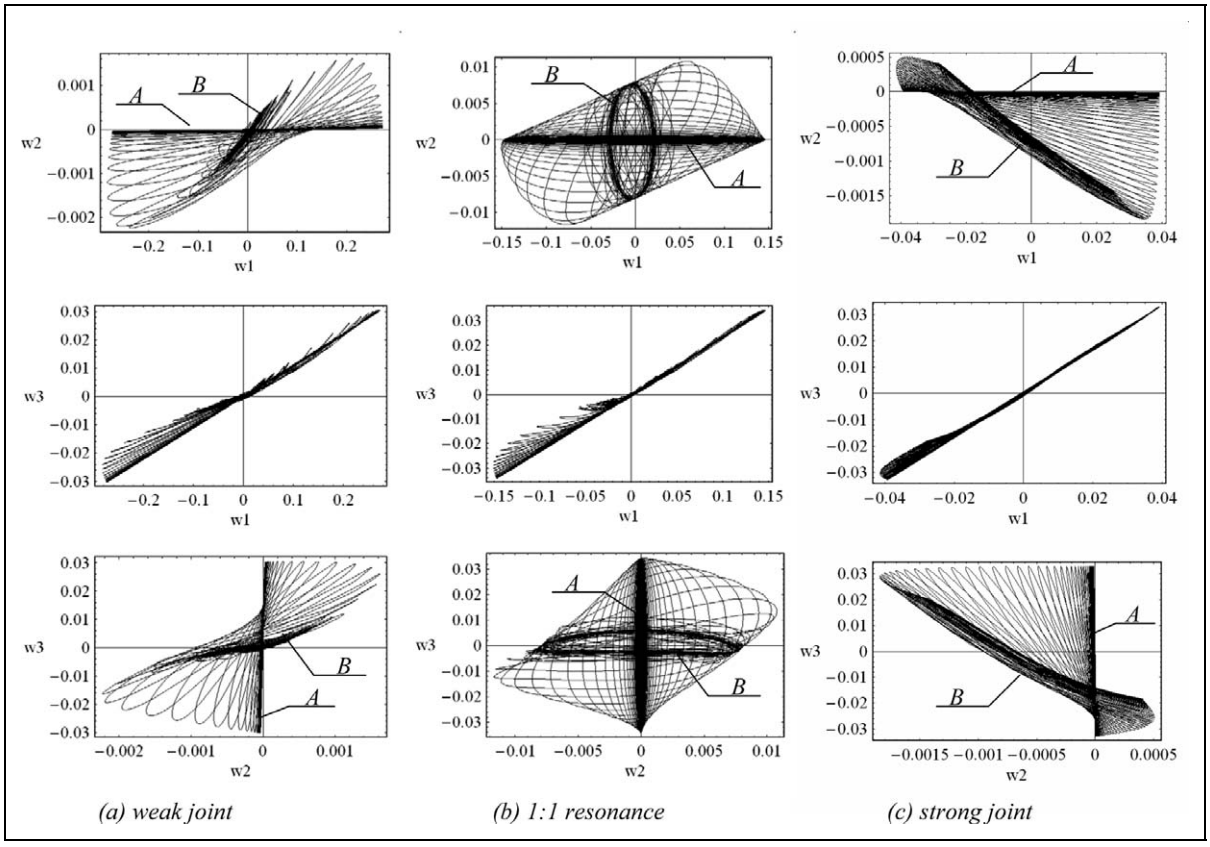


**Figure 17.** Projections of the system trajectory on the original generalized coordinate planes under the developing fracture condition and loading $p_1 = 0.1 \sin \omega_1 t$, $p_2 = p_3 = 0$; no elastic foundation assumed.

interval 100, after which the left side of the joint becomes almost completely separated from the beam. In real applications though, the duration of crack formation depends on the number of cycles and the level of vibration amplitude. The corresponding modeling is rather outside the scope of present study. The proposed model given by equation (29) is applied for the purpose of illustrating how the system's dynamic response is affected by crack formation in the time and frequency domains.

First, a series of numerical simulations dealing with different stiffnesses of joints under the no-elastic-foundation condition ($k_f = 0$) is performed. In all cases, the model is excited by the harmonic loading in equation (27) with the first mode frequency as follows: $p_1(t) = 0.1 \sin \omega_1 t$, $p_2(t) = 0.0$, and $p_3(t) = 0.0$. Therefore, the spatial shape of loading is given by one-half of a sine wave that corresponds to the first mode of the beam with no joint. It is seen from equations (20), (25), and (27) that this loading will directly excite the first and third modes of the beam with joint. However, the first mode will be predominantly excited due to the above choice for input frequency. In addition, there is no direct excitation of the second mode, which may only oscillate as a result of nonlinear modal interaction after the initiation of a crack.

The results of simulations are illustrated in Figures 10 through 13. In particular, Figure 10 displays a series of system trajectory projections on different configuration planes for three different cases of the joint strength. The diagrams clearly demonstrate the fact that the system changes its attractor (from A to B) as the crack develops but in a different way for different joint strengths. In the resonance case (b) where $\omega_1 = \omega_2$, the second mode has eventually the largest amplitude with a specific phase shift $\pi/2$ that is reflected by the elliptic shape of the attractor's projection on the $q_1 q_2$ plane as shown by the top diagram of Figure 10(b). Below and above resonance, the projections of the final attractor on the same configuration plane are rather close to straight lines, however, directed in a different way: in-phase and out-of-phase for weak and strong joints, respectively. This resembles a typical oscillator behavior passing through the resonance. In our case, the"oscillator'' is represented by the second mode, whereas the excitation comes mostly from the first mode subjected to the direct resonance loading.

The second row in Figure 10 displays projections on the $q_1 q_3$ plane. Since the second mode does not participate in the projection, then the resonance with the second mode has a minor effect on the projection shapes as one compares cases (a) and (b) in the second row. Case (c) slightly differs

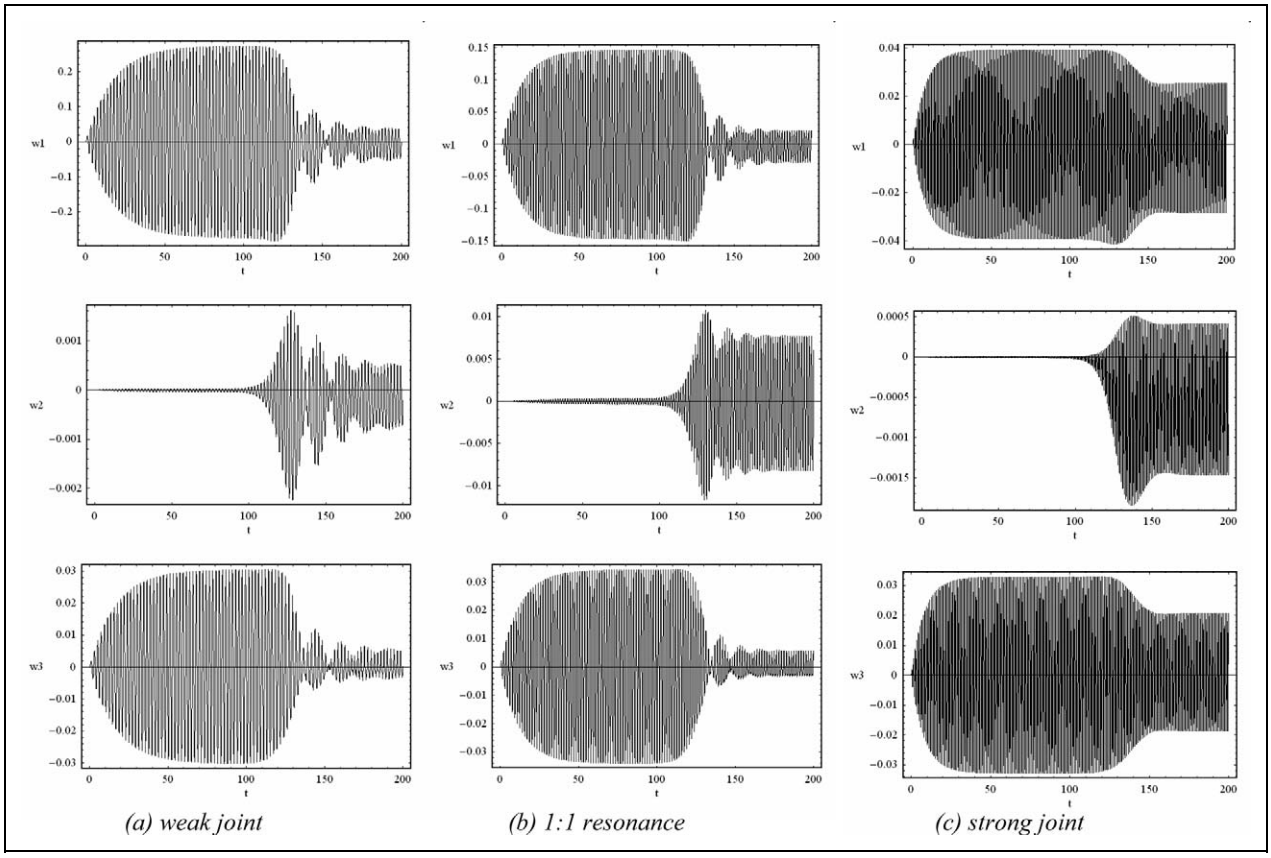


**Figure 18.** Original generalized coordinate time histories under the conditions of Figure 17.

though because of effective structural changes in the model due to the stiffer joint. Finally, the third row shows $q_2q_3$ projections. The transition to the final (developed crack) attractors has a quite chaotic character in cases (a) and (b). Still, it is seen that the path is more regular in the case of a stiffer joint (c).

Related to Figure 10 are response time histories and corresponding spectrograms for individual modes. These are shown in Figures 11 through 13 for the three different cases of Figure 10. The short windowed Fourier spectrograms are generated by the''specgram'' procedure built into the MATLAB-7 package. In both temporal and spectral representations, the developing fracture is clearly seen through the growing amplitudes of secondary modes as well as the spectral widening. Once again, more regularity is observed in the case of the stronger joint. In all three cases shown in Figures 11 through 13, it is seen that near $t \approx 100$ an energy transfer takes place from the first mode, which is directly excited, to the other two modes. The energy transfer is attributed to the nonlinearity created by crack formation.

The next series of diagrams shown in Figures 14 through 16 deals with the loading of the same spatial mode shape, but with an excitation frequency which is equal to the second linear mode frequency. In this case the loading components are: $p_1(t) = 0.1 \sin \omega_2 t$, $p_2(t) = 0.0$, and $p_3(t) = 0.0$. In other words, this case deals with the indirect excitation to the second mode through the symmetric modes. In contrast to the previous case, due to the resonance with the second mode, there is no significant energy exchange with the first mode. In addition, the influence of a foundation is considered in this case. The internal resonance, $\omega_1 = \omega_2$, leads to quite significant qualitative changes in trajectory projections as follows from the comparison of columns (a) and (b) in Figure 14. Also, the internal resonance results in a stronger dynamic complexity in both temporal and spectral characteristics of motion as from the comparison of Figures 15 and 16. Note that the third mode $q_3(t)$ has a zero initial condition, however, it directly excited as reflected by equations (20), (25), and (27). Accordingly, Figure 15 displays a nonzero amplitude in the transient period.

A common feature displayed in Figures 10 through 16 is the evolution of the dynamic behavior of the normal modes as the crack develops. The adopted model for a crack exhibits asymmetric nonlinear stiffness characteristics. As a result, the asymmetry observed in time history records and configuration planes can also be viewed as an indication of fracture formation in the joint.

Using the coordinate transformation, (23), gives the corresponding configuration plane and time history representations of the dynamics in terms of the original

geometrical modes as shown in Figures 17 and 18, respectively. It follows from expressions (23) that the second mode is not affected by the transformation, whereas the first and third modes are coupled due to the presence of a joint localized at the middle of the beam. Nevertheless, in most cases, except that shown in Figure 14, the first mode appears to be the major energy receiver from the external loading regardless of the type of coordinates. As a result, the diagrams represented on planes $q_1q_2$ and $w_1w_2$ in Figures 10 and 17, respectively, look qualitatively similar, but all other planes are quite different.

Note that the spatiotemporal modeling of loading given by equation (20) has been specifically chosen for the purpose of crack detection. This can be experimentally implemented in the lab by appropriate actuators. Furthermore, the present study focused on specific features of nonlinear dynamics based on three degrees of freedom. Had the analysis been extended to a more comprehensive structural model, it could result in describing other features unrelated to the crack detection methodology described in this work. From the standpoint of the strength of materials and design issues, finite element software packages have already been developed as outlined in the introduction.

## 7. Conclusion

According to the overview presented in the introduction, the design of T-joints in ship structures is based on experimental measurements of failure loads, fracture and fatigue characteristics. These also have been predicted using finite element analysis and other numerical algorithms. However, during ship navigation in violent ocean waves, it is imperative to have some nondestructive tools that are capable of identifying crack formation, which may occur at weak locations such as joints and fasteners. This work has proposed a reduced order model for T-joints of elastic beams admitting the possibility of crack formation. Based on the analytical modeling and numerical simulations, different qualitative changes of the dynamics due to crack formation have been predicted in the configuration plane, temporal and spectral representations.

The normal mode frequencies of the main structure have been found to be affected by the presence of the crack. Under external dynamic loading with a frequency close to the first mode frequency, the development of the crack has been revealed by the evolution of the configuration plots on the planes. In the absence of a crack the attractor is essentially a straight line and then rotates with time as the crack develops. Another tool for detecting crack formation is through the frequency content evolution of each mode represented by spectrogram plots. Therefore, multiple signal processing tools could be employed for the nondestructive diagnostics of joints, where damage may be hidden under layers of material.

## Acknowledgements

This work is supported by a grant from ONR under Award No: N00014-08-1-0647. Dr Kelly B. Cooper is the Program Director.

## References

Andreaus, U., Casini, P., and Vestroni, F., 2007,"Non-linear dynamics of a cracked cantilever beam under harmonic excitation,'' *International Journal of Non-Linear Mechanics* **42(3)**, 566-575.

Bhattacharya, B., House, J. R., Mercy, S. E., and Tomlinson, G. R., 2000,"Low- and high-frequency energy-absorbing composite joints,'' in *Proceedings of the SPIE - The International Society for Optical Engineering*, Newport Beach, CA, Vol 3989, pp. 152-158.

Bickford, J. H., 1990, *An Introduction to the Design and Behavior of Bolted Joints*, 2nd edition, Marcel Dekker, New York.

Blake, J. I. R., Shenoi, R. A., and Turton, T., 2001,"Progressive damage analysis of tee joints with viscoelastic inserts,'' *Composites Part A: Applied Science and Manufacturing* **32(5)**, 641-653.

Brunner, A. J. and Paradies, R., 2000,"Comparison of designs of CFRP-sandwich T-joints for surface-effect ships based on acoustic emission analysis from load tests,'' American Society for Testing and Materials (ASTM) Special Technical Publication Number 1383, pp. 366-381.

Burchardt, C., 1995,"Load conditions and stresses for T-joints in planning ships,'' in *Sandwich Construction*, Allen, H. G. (ed.), Southampton, EMAS 3(2), pp. 613-623.

Butcher, E. A., 1999,"Clearance effects on bilinear normal mode frequencies,'' *Journal of Sound and Vibration* **224(2)**, 305-328.

Butcher, E. A. and Lu, R., 2007,"Order reduction of structural dynamic systems with static piecewise linear nonlinearities,'' *Nonlinear Dynamics* **49(3)**, 375-399.

Chati, M., Rand, R., and Mukherjee, S., 1997,"Modal analysis of a cracked beam,'' *Journal of Sound and Vibration* **207**, 249-270.

Chen, S. and Shaw, S., 1996,"Normal modes for piecewise linear vibratory systems,'' *Nonlinear Dynamics* **10**, 135-163.

Cheng, S. M., Swamidas, A. S. J., Wallace, W., and Wu, X., 1999,"An experimental investigation of tubular T-joints under cyclic loads,'' *Journal of Offshore Mechanics and Arctic Engineering* **121(3)**, 137-143.

Dharmawan, F., Li, H. C. H., Herszberg, I., and John, S., 2008,"Applicability of the crack tip element analysis for damage prediction of composite T-joints,'' *Composite Structures* **86(1-3)**, 61-68.

Dharmawan, F., Thomson, R. S., Li, H., Herszberg, I., and Gellert, E., 2004,"Geometry and damage effects in a composite marine T-joint,'' *Composite Structures* **66**, 181-187.

Dodkins, A. R., Shenoi, R. A., and Hawkins, G. L., 1994,"Design of joints and attachments in FRP ships' structures,'' *Marine Structures* **7(2-5)**, 365-398.

Eksik, O., Shenoi, R. A., Moy, S. S. J., and Jeong, H. K., 2007a,"Experiments on top-hat-stiffened panels of fiber-reinforced-plastic boat structures,'' *Marine Technology* **44(1)**, 1-15.

Eksik, O., Shenoi, R. A., Moy, S. S. J., and Jeong, H. K., 2007b,"Finite element analysis of top-hat-stiffened panels of fiber-reinforced-plastic boat structures,'' *Marine Technology* **44(1)**, 16-26.

Hawkins, G. L., Holness, J. W., Dodkins, A. R., and Shenoi, R. A., 1993,"Strength of bonded tee-joints in FRP ships,'' *Plastics, Rubber and Composites Processing and Applications* **19(5)**, 279-284.

Ibrahim, R. A. and Pettit, C. L., 2005,"Uncertainties and Dynamic Problems of Bolted Joints and other Fasteners,'' *Journal of Sound and Vibration* **279(3-5)**, 857-936.

Jiang, D., Pierre, C., and Shaw, S., 2004,"Large-amplitude non-linear normal modes of piecewise linear systems,'' *Journal of Sound and Vibration* **272**, 869-891.

Junhou, P. and Shenoi, R. A., 1996,"Examination of key aspects defining the performance characteristics of out-of-plane joints in FRP marine structures,'' *Composites Part A: Applied Science and Manufacturing* **27(2)**, 89-103.

Kesavan, A., Deivasigamani, M., John, S., and Herszberg, I., 2006,"Structural health monitoring of composite T-joints for assessing the integrity of damage zones,'' in *Proceedings of the SPIE on Smart Structures and Materials: Smart Sensor Monitoring Systems and Applications - The International Society for Optical Engineering*, San Diego, CA, Vol. 6167, 61670E -1-12.

Kumari, S. and Sinha, P. K., 2002,"Finite element analysis of composite wing T-joints,'' *Journal of Reinforced Plastic Composites* **21**, 1561-1585.

Li, H. C. H., Dharmawan, F., Herszberg, I., and John, S., 2006,"Fracture behavior of composite maritime T-joints,'' *Composite Structures* **75(1-4)**, 339-35.

Maneepan, K., Jeong, H. K., and Shenoi, R. A., 2005,"Optimization of FRP top-hat stiffened single skin and monocoque sandwich plates using genetic algorithm,'' in *Proceedings of the 15th International Offshore and Polar Engineering Conference (ISOPE-2005)*, Seoul, Korea, Vol. 2005, pp. 513-518.

Mouritz, A. P., Gellert, E., Burchill, P., and Challis K., 2001,"Review of advanced composite structures for naval ships and submarines,'' *Composite Structures* **53**, 21-41.

Nwosu, D. I., Swamidas, A. S. J., and Guigne, J. Y., 1996,"Dynamic response of tubular T-joints under the influence of propagating cracks,'' *Journal of Offshore Mechanics and Arctic Engineering* **118(1)**, 71-78.

Phillips, H. J. and Shenoi, R. A., 1998,"Damage tolerance of laminated tee joints in FRP structures,'' *Composites Part A: Applied Science and Manufacturing* **29(4)**, 465-478.

Phillips, H. J., Shenoi, R. A., and Moss, C. F., 1999,"Damage mechanics of top-hat stiffeners used in FRP ship construction,'' *Marine Structures* **12(1)**, 1-19.

Pilipchuk, V. N., 2009,"Closed form periodic solutions for piecewise-linear vibrating systems,'' *Nonlinear Dynamics*, http://dx.doi.org/10.1007/s11071-009-9469-0

Read, P. J. C. L. and Shenoi, R. A., 1999,"Fatigue behavior of single skin FRP tee joints,'' *International Journal of Fatigue* **21(3)**, 281-296.

Richtmyer, R. D., 1985, *Principles of Advanced Mathematical Physics*, Vol. 1, Springer, Berlin.

Shenoi, R. A. and Hawkins, G. L., 1992,"Influence of material and geometry variation on the behavior of bonded tee connections in FRP ships,'' *Composites* **23**, 335-345.

Shenoi, R. A. and Hawkins, G. L., 1995,"Investigation into the performance characteristics of top-hat stiffener to shell plating joints,'' *Composite Structures* **30(1)**, 109-121.

Shenoi, R. A., Read, P. J. C. L., and Jackson, C. L., 1998,"Influence of joint geometry and load regimes on sandwich tee joint behavior,'' *Journal of Reinforced Plastics and Composites* **17(8)**, 725-740.

Stickler, P. B. and Ramulu, M., 2001,"Investigation of mechanical behavior of transverse stitched T-joints with PR520 resin in flexure and tension,'' *Composite Structures* **52(3-4)**, 307-314.

Stickler, P. B. and Ramulu, M., 2002,"Parametric analyses of stitched composite T-joints by the finite element method,'' *Materials and Design* **23(8)**, 751-758.

Stickler, P. B. and Ramulu, M., 2006,"Damage progression analyses of transverse stitched T-joints under flexure and tensile loading,'' *Journal of the Japan Society of Composite Materials: Advanced Composite Materials* **15(2)**, 243-261.

Theotokoglou, E. E., 1997,"Strength of composite T-joints under pull-out loads,'' *Journal of Reinforced Plastics and Composites* **16(6)**, 503-518.

Theotokoglou, E. E., 1999,"Study of numerical fracture mechanics analysis of composite T-joints,'' *Journal of Reinforced Plastics and Composites* **18(3)**, 215-223.

Theotokoglou, E. E. and Moan, T., 1996,"Experimental and numerical study of composite T-joints,'' *Journal of Composite Materials* **30(2)**, 190-209.

Toftegaard, H. and Lystrup, A., 2005,"Design and test of lightweight sandwich T-joint for naval ships,'' *Composites: Part A: Applied Science and Manufacturing* **36(8)**, 1055-1065.

Turaga, U. V. R. S. and Sun, C. T., 2000,"Failure modes and load transfer in sandwich T-Joints,'' *Journal of Sandwich Structures and Materials* **2(3)**, 225-245.

Vestroni, F., Luongo, A., and Paolone, A., 2008,"A perturbation method for evaluating nonlinear normal modes of a piecewise linear two-degrees-of-freedom system,'' *Nonlinear Dynamics* **54(4)**, 379-393.

Zhou, D. W., Louca, L. A., and Saunders, M., 2008,"Numerical simulation of sandwich T-joints under dynamic loading,'' *Composites: Part B: Engineering* **39**, 973-985.